Oil Shale, 2023, Vol. 40, No. 2, pp. 91–114
doi: https://doi.org/10.3176/oil.2023.2.01
ISSN 0208-189X

Pore and fracture scale characterization of oil shale at different microwave temperatures

Longfei Zhao[(a)], Yao Cheng[(b)*], Yongli Zhang[(a)]

[(a)] School of Mechanics and Engineering, Liaoning Technical University, Fuxin 123000, China
[(b)] College of Innovation and Practice, Liaoning Technical University, Fuxin 123000, China

Received 10 November 2022, accepted 14 April 2023, available online 10 May 2023

Abstract. *The spatial complexity of oil shale systems is manifested by microstructure, pore space randomness and extensive heterogeneity. A microwave pyrolysis device developed for this study was used to pyrolyze oil shale, and the microstructure before and after pyrolysis was visually examined and quantified. The internal structure of the rock and the extent of pore and fracture expansion are more accurately determined in this way. The microstructure of oil shale at different temperatures before and after microwave pyrolysis is identified by X-ray microcomputed tomography (μCT) with automatic ultra-high-resolution scanning electron microscopy (SEM), to observe the heterogeneous state of oil shale on 2D and 3D scales and define the distribution of internal pores and fractures by post-processing μCT visualization. The study found that fractures sized from microns to millimeters along with pore fractures were observed at increasing microwave temperatures. The fractures gradually expanded with increasing temperature in the direction of horizontal or vertical laminae and generated a more connected pore network. The kerogen gradually decreased with a rise in temperature. The porosity increased from 0.26% to 13.69% at the initial temperature. This research is essential for the qualitative as well as quantitative analysis of the internal structure of oil shales under microwave radiation.*

Keywords: *Fushun oil shale, microwave pyrolysis, digital core, SEM, μCT.*

* Corresponding author: e-mail *yaoyao9873@163.com*

1. Introduction

Due to the significant increase in energy demand, countries are committed to oil shale as an alternative source of petroleum. Oil shale is widely used in electrical power generation and the petrochemical and construction industries as an alternative to conventional oil and gas, thanks largely to the accessibility of its huge reserves [1, 2]. Global shale oil resources are up to 450 billion tons, with the United States, China and Russia having the world's largest oil shale reserves [3]. In China, the vigorous development of the oil shale industry guarantees the country's national energy security. Oil shale is a sedimentary rock with a mineral skeleton, and may contain the roots of caseous species and small amounts of minerals. Shale oil is the product of pyrolysis, which comprises a series of physical and chemical reactions, e.g., moisture volatilization, thermal rupture of laminae and pyrolysis of casein, forming pores and fractures in the rock [4–6]. The latter thereafter play a crucial role in the transport of the pyrolytic products.

Based on the method used, oil shale heating is classified into conduction heating, convection heating and radiative heating [7–9]. Microwave radiation has been proposed as a method for heating rocks [10] and coal [11] due to its advantages of fast heating rate and high energy utilization. Many studies have applied radiative heating to examine the evolution of fine structure and permeability during the pyrolysis of oil shale. Microwaves heat the sample volumetrically and overcome the problem of low thermal conductivity and uneven heating. It has been found that dry distillation of oil shale by microwave radiation produced shale oil that was compositionally superior to that obtained by conventional dry distillation, with a higher proportion of light hydrocarbons and lower sulfur and nitrogen content [12]. Measurement established that the dielectric values of oil shale at different temperatures increase significantly at 400–500 °C, and both the density and dielectric constant decrease with increasing shale oil production [13]. Rapid microwave warming causes distillation, viscosity reduction and fracturing reactions associated with kerogen decomposition, as well as rock decomposition, beyond a certain temperature. It was also demonstrated that although the dielectric constant of oil shale is low, the addition of materials such as iron oxide or iron chloride enhances microwave absorption [14].

In the process of oil shale reservoir evaluation, one of the core tasks of quantitative characterization and analysis of pore structure is to study the microscopic properties of dense reservoirs because of their profound impact on oil and gas development in oil shale. Of these, the pore geometry, size and distribution, and the distribution and relationship of fractures and microfractures have a great effect on the physical properties of the reservoir rocks. Many experiments have been conducted to evaluate the pore structure of oil shale after conventional heating, using piezometric porosimetry [15], nitrogen adsorption-desorption isotherms [16] and scanning electron

microscopy (SEM) [17]. However, few studies have been reported describing visualization of the pore network and the effect of fracture formation and porosity quantification in oil shale after microwave radiation. The volume and specific surface area of pores in oil shale have been calculated by nitrogen adsorption/desorption [18, 19]. This method does not visually observe individual or connected pores, however. Since pore fractures in oil shale are the main transport pathways for oil and gas, observation of the location, distribution and geometry of internal pores and fractures in three dimensions after microwave pyrolysis are particularly useful [20].

Conventional optical microscopy and SEM are used to watch the superficial distribution of organic matter (OM) and minerals, but do not reveal the internal microstructure or the pore network [21]. The development of pores and microfractures during pyrolysis of oil shale is due to the uneven heating of its internal structure caused by the strong heterogeneity of the rock during heating. X-ray microcomputed tomography (μCT) imaging effectively analyzes the distribution of internal pores and fractures in the rock, and is a powerful tool for visualizing and quantifying the internal structure of geological materials, particularly in the study of pore structure [22, 23]. These non-destructive scans provide three-dimensional imaging at the micrometer or nanometer scale, as required. In the context of the present study, digital core reconstruction after μCT scanning produces information about the spatial distribution of organic and inorganic minerals, and enables observation of the changes in pore space after pyrolysis. Quantitative analysis of basic pore geometry properties of oil shale (e.g., pore size, shape, tortuosity and fractal dimensions) provide insight into the pore network space and the distribution of fractures, as well as the transport behavior of oil and gas during pyrolysis. A study using high-temperature water vapor to pyrolyze oil shale, followed by its three-dimensional volume reconstruction, found that increased temperature resulted in a more obvious cracking along the laminae surfaces, and that the number and length of cracks increased rapidly [24]. Another study showed through micro-CT scans that inorganic minerals within the oil shale break down under the action of microwave radiation, reconstituting them into new minerals while increasing the surface area and volume of oil shale. In addition, the fracture extension evolution of oil shale during uniaxial compression was also discovered using the micro-CT technique, which proved that the fracture network of oil shale is one of the critical factors for enhanced oil and gas recovery.

The present study investigated the effect of different temperatures (350, 400, 500 and 600 °C) at a microwave power of 800 W, followed by SEM description of the surface and mineral morphology of oil shale. The study ascertained that 350 °C is the critical temperature of pyrolysis at which oil shale starts to pyrolyze and the phase change of internal kerogen occurs. 600 °C was established to be the final temperature of oil shale pyrolysis at which the internal kerogen reacts completely and produces a relatively large amount

of oil and gas. The degree of porosity and anisotropy of the microwave-heated oil shale was quantified by μCT scanning. Since fractures determine the source/sink of oil and gas diffusion in the oil shale matrix, fractures and microfractures were identified from grayscale μCT images, and the direction of oil and gas diffusion obtained from the 3D fracture framework followed by the use of digital core technology. The visualization of pores and fractures enabled the fractures and microfractures to be examined separately. The experimental results provide a reference for both the microstructural changes in oil shale and the transformation of organic matter when subjected to microwave radiation.

2. Experiment

2.1. Sample preparation

In this study, oil shale from the Fushun area in China was used for testing. Industrial and Fischer oil content analyses indicate an oil content of 2–13% (average 5.5%). Table shows the oil content to be 6.02%, while the high content of OM implies its high research value. The Fushun oil shale originates from Eocene lake deposits. The Fushun mine is an open-pit mine; oil shale samples were extracted from the surface of the mine and immediately sealed. To minimize the influence of non-homogeneity in the rock and differences between individual samples, holes were drilled on the vertical bedding of the same oil shale to obtain cylindrical samples 20 mm in diameter and 20 mm height. The oil shale samples at different temperatures (25, 350, 400, 500, 600 °C) were then scanned by SEM and μCT to investigate the influence of temperature on the samples' surface morphology and internal structure.

Table. Industrial and Fischer analyses of Fushun oil shale

Parameter analysis	Industrial analysis				Fischer analysis			
	Moisture	Ash	Volatile matter	Fixed carbon	Oil yield	Water yield	Residue	Gas + loss
Yield, %	2.88	77.19	17.76	2.17	6.02	4.44	85.60	3.94

Microwave heating, as an unconventional technical means, has the characteristics of fast heating speed, volume heating, selective heating, low energy loss, etc. So the experiments were carried out using a purpose-built microwave pyrolysis device (Fig. 1) to apply different microwave parameters, including heating time, output power and reaction temperature. Oil shale was

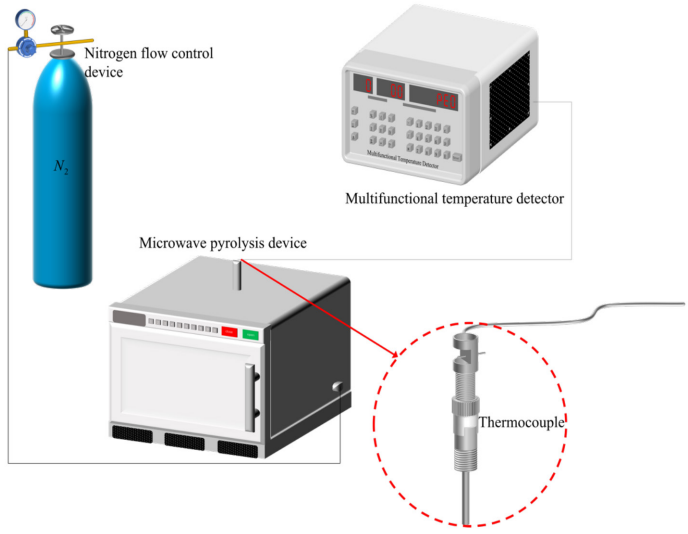

Fig. 1. Experimental microwave heating system.

subjected to microwave irradiation. The semi-coke prepared at the laboratory was added to improve the heating efficiency. For each sample, 2.5 g of semi-coke and oil shale was placed in a sealed device containing ceramic fibers.

The microwave heating system mainly consists of a magnetron and a waveguide with a maximum frequency of 2450 MHz and a maximum output power of 1200 W, respectively. Ceramic fibers were wrapped around the sample and the sample chamber was filled with nitrogen to ensure that no oxygen entered the device. While nitrogen is injected into the microwave unit, oil shale begins to pyrolyze and the resulting oil and gas can only be discharged from the rear heat sink by mixing with nitrogen due to the limitations of the unit. The thermocouple is inserted into the upper part of the device, and the thermocouple is fixed to the microwave unit housing by using metal bolts, to ensure that the thermocouple forms an integral part of the microwave metal housing, thus increasing the accuracy of the measurement. It is also possible to measure temperatures from 350 to 600 °C in real time. The oil shale samples were subjected to microwave radiation for different times, while one oil shale specimen was placed under each temperature band, and the oil shale temperature gradually increased with increasing microwave radiation time. Thermocouples are installed in the upper part of the microwave oven. The thermocouple is secured using nuts so that this device forms an integral part of the microwave oven, ensuring the integrity of the system and avoiding it from heating when the temperature rises to a specific level to ensure that oil shale is pyrolyzed at a required temperature.

In the laboratory procedure, nitrogen was injected and a specific power was set at 800 W to heat the sample for the required period of time, observing at the same time the change of temperature. When the required temperature was reached, it was held for 1 hour to allow full pyrolysis. At the end of each experiment, the equipment was turned off and allowed to cool naturally to room temperature, and the sample was then removed (Fig. 2). Subsequently the SEM and μCT scans of the sample were produced, to observe the pore fracture and fracture alterations, as well as spatial structural changes inside the oil shale. This is important from the viewpoint of oil and gas transport within the oil shale sample.

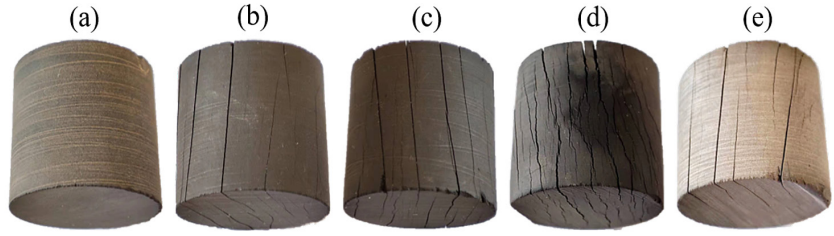

Fig. 2. Images of pyrolyzed oil shale samples at different temperatures: (a) 25 °C; (b) 350 °C; (c) 400 °C; (d) 500 °C; (e) 600°C.

2.2. Scanning electron microscopy

Scanning electron microscopy is commonly used as a direct method for distinguishing pore type, morphology and radius of the sample, it also quickly and visually characterizes the distribution of kerogen therein [25]. SEM scans were used to watch the distribution of organic matter and minerals in the oil shale sample to examine the decomposition of kerogen on its surface at different temperatures at specific power. The surface morphology and distribution of minerals were obtained as two-dimensional images of the oil shale sample. The surface morphology and distribution of OM were shown more clearly by electron beam sputtering and gold plating, and the induced pores, fractures and directions after microwave irradiation were ascertained by digital image analysis. The working voltage of SEM was set to 10 kV; in general, better image resolution is obtained at higher voltages. High acceleration voltage may be used when the sample has good conductivity and will not be damaged by the electron beam.

The magnification of the sample was 1000x, with the working distance set to 12.8 mm. These were found after several trials to be the optimal experimental parameters. When the working distance is increased, the beam spot on the surface of the sample becomes larger and resolution decreases, the aperture angle decreases and the depth of the field increases. SEM was used to obtain high-precision images of the surface morphology to determine the

location and distribution of pore fractures and organic matter in the samples subjected to different temperatures. In conducting SEM experiments, beam electron polishing is performed and the location of the oil shale samples to be subjected to these experiments for repeated positioning is marked. SEM enables the specimens to be heated at each temperature point to find the right position in the experiments, to ensure that they can be irradiated on the same oil shale surface.

2.3. μCT scan and core reconstruction

2.3.1. μCT scanning and processing

Considering its rapid development, μCT is increasingly used in various industries [26, 27]. It is the method commonly used to determine the internal conditions of oil shale in a non-destructive way, and shows the interior of the sample microscopically without destroying its shape or size, revealing the number and distribution of pores and fractures. Experiments were performed using the μCT255kvFCB micro-scanning system at Taiyuan University of Technology. The volumetric reconstruction of oil shale in the original state as well as after pyrolysis was performed at 180 kV and 150 μA, and internal microspatial structures such as pores and fractures were analyzed.

The scan data was then transformed into 1500 two-dimensional gray-scale slice images. For volume reconstruction after CT scanning, a voxel (volumetric pixel) size of 8 μm was selected. Figure 3 shows the location and distribution of and color difference between the mineral matrix and fractures in the slice

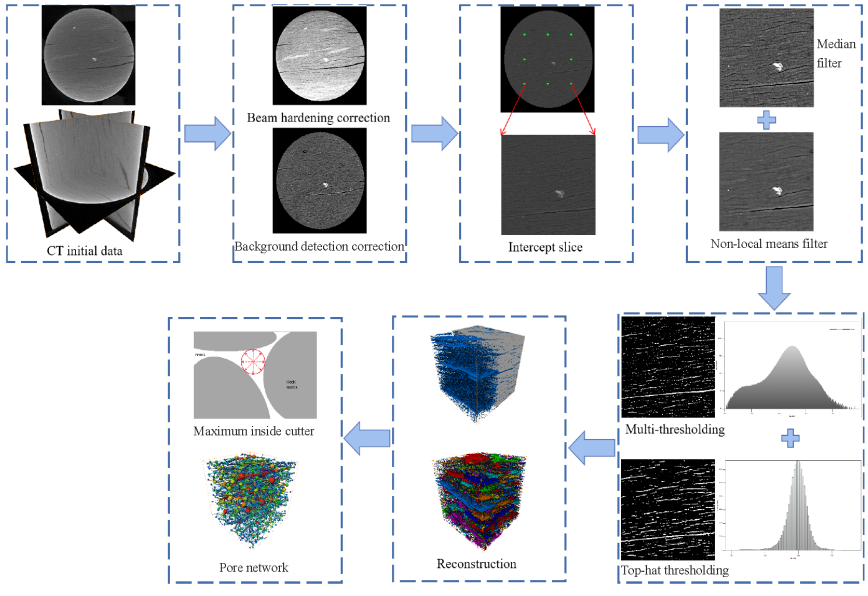

Fig. 3. CT processing flow chart.

images. Pore fractures appear to be black; the white color represents high-density mineral grains. The gray areas represent lower-density clay minerals and caseous roots. However, as the said minerals and roots are extremely similar in color, it is difficult to make any distinction between them.

In the μCT-aided volume reconstruction, the energy spectral rays continuously pass through the sample, the lower-energy rays are absorbed and the higher-energy rays pass through. For any given material, the attenuation coefficient decreases with increasing photon energy, so that a higher-energy beam penetrates further. As the beam passes through the attenuating material, the significantly lower energy is absorbed. This reduces the amount of low energy in the overall beam spectrum ("hardened" beam), causing less attenuation of the beam as it penetrates further into the material. This effect is seen as a white aperture around the image, which can be eliminated using beam hardening correction [28] to iteratively optimize the agreement between re-projections by reconstructing the data for the actual object and its projection.

Image noise may create large errors in segmentation; therefore, the direct application of the threshold value may well lead to poor segmentation. There are three ways to solve this problem: a) reducing the noise of grayscale data before segmentation; b) reducing the morphological noise of binarized data after segmentation; c) using a noise-resistant segmentation method, which allows more flexibility than filtering the data upon filtering grayscale images after threshold segmentation. For better fracture detection, median filtering by non-local mean filtering reduces impulse noise, and fracture images are reduced to a linear shape using a kernel smoother. This technique is more suitable for segmenting fractures and maintaining their width in 2D images.

As hydrocarbons diffuse from the rock matrix into the fractures, in experiments, the spatial location of the fractures had to be identified prior to identifying the latter themselves. Traditional fracture identification methods, e.g., watershed segmentation, do not identify microfractures effectively [29]. However, microfractures are the pathways for hydrocarbon diffusion in the rock matrix [30]. To more accurately identify them, a new image processing method is needed. Multi-threshold segmentation [31] and the top-hat transform [32] were applied to each slice image to completely segment fractures, including pore fractures, and obtain a 3D digital model that reflects the real situation within the rock.

In multi-threshold segmentation, an image histogram shows the number of times each voxel value occurs, as well as the current partition of the gray value range. Two peaks are identified and the corresponding threshold or segmentation boundary is set at the minimum between consecutive peaks, which is then the left-hand peak to the lowest point.

In the top-hat thresholding algorithm, different combinations of open and closed operations constitute the open and closed top-hat operator. The principle of the open top-hat operator is that it eliminates brightest details in the grayscale image by subtracting the open operation result from the original

image, thus increasing the brightness of the target region. The closed top-hat operator principle consists in that it eliminates the darkest details in the grayscale image by subtracting the original image from the result of the closed operation, thus reducing the brightness outside the target area. The closed operation was used in this study to extract the pore fissures and microfissures that could not be extracted during multi-threshold segmentation.

2.3.2. Microscopic observation and analysis

The internal three-dimensional pore space in oil shale is the main seepage channel for oil and gas transport. In order to study the true distribution of three-dimensional pore space and pore volume after pyrolysis, a three-dimensional digital core was now constructed from the μCT scans, which is an important aspect of in situ production of oil shale by microwave heating. The oil shale samples were subjected to CT scanning, and a total of 1500 slices were scanned out of each oil shale sample. Due to insufficient computer capacity, a sample of a size of 445 × 445 × 445 voxels was selected as a representative basic volume (REV) size when the μCT data volume cut was performed on the sample. The features of pore fractures, microfractures and cracks were extracted from the threshold-segmented samples. The results are shown in Figure 4. For the preprocessed grayscale slices of oil shale the fast Fourier transform (FFT) filtering and non-local median filtering were used, in which the slices were continuously cut perpendicular to the laminae [33]. The grayscale images of the oil shale samples of interest were selected using a region-of-interest (ROI) approach to ensure that the computer hardware could properly operate while guaranteeing the accuracy of the pore fracture microstructure calculations.

Due to the structure and irregularities of pores in oil shale samples, no uniform standard is used for their statistical analysis; the porosity and permeability in different directions in the samples are established to analyze the distribution of fractures, including pore fractures.

The surface porosity and total porosity can be given by Equations (1) and (2):

$$\phi_i = \frac{V_{\phi i}}{V_i}, \tag{1}$$

where ϕ_i is the surface porosity; $V_{\phi i}$ is the pore volume at voxel i distance; V is the volume at voxel i distance.

$$\phi = \frac{V_\phi}{V}, \tag{2}$$

where ϕ is the total porosity, %; V_ϕ is the volume of pore space, μm^3; V is the total volume, μm^3.

2.3.3. Equivalent pore-network modeling

For the geometric system of pore space shown in Figure 6, the share of pore fracture and throat size was calculated at different temperatures using a maximum searching algorithm. The use of a two-step finding algorithm to determine the maximum sphere corresponding to each pore voxel has been reported to greatly improve computational efficiency [34], as did a tree-like structure and clustering algorithm to determine the pore and throat channels in the digital core space based on the radius and volume of the maximum sphere. As shown in Figure 5, for a digital core, the radius of the hole is defined as the maximum inner tangent sphere radius; the length of the throat channel is defined as the maximum length at the connection of two chains sphere inside it. The inner tangent sphere and throat corresponding to each pore voxel in the pore space is obtained, and after determining the precise location of the pore and fracture space, a small sphere is positioned at the center of each and their volumes are continually increased until they are in contact with and tangential to the wall of the hole. Therefore, it relies on the maximum possible size of each sphere; the largest spheres formed by the numerous pore fissures and fractures are then correlated. The algorithm thereafter distinguishes between the major and minor spheres. The spatial regions corresponding to the pore cavity and the throat channel are identified and distinguished in accordance with the topology of the pore fissure or fracture, and the pore topology parameters are precisely quantified.

In building the equivalent sphere, the largest sphere when the equivalent sphere is in contact with the solid skeleton is selected for calculation:

$$R = \mathrm{dist}^2(C, V_g) = (x_g - x_c)^2 + (y_g - y_c)^2 + (z_g - z_c)^2,\ V_g \in S_g,\ C \in S, \quad (3)$$

where R is the maximum ball radius, μm; C is the center of the pore, μm; V_g is the skeleton of the rock; $x_g y_g z_g$ are the locations of pore centers, μm; $x_c y_c z_c$ are the rock skeleton locations, μm; S_g is the rock skeleton voxel point; S is the pore space voxel point.

When establishing the equivalent howl length, the howl length is defined as the total howl length minus the length of the two pores:

$$l_t = l_{ij} - l_i - l_j\ , \quad (4)$$

where l_t is the throat length, μm; l_{ij} is the total throat length, μm; l_i, l_j are the lengths of two pore spaces, μm.

$$l_i = l_i^t(1 - \alpha \frac{r_t}{r_i})\ , \quad (5)$$

$$l_j = l_j^t(1 - \alpha \frac{r_t}{r_j})\ , \quad (6)$$

where l_i^t, l_j^t are the distances from the center of the pore sphere i, j to the center of the throat sphere, respectively; $r_i r_j r_t$ are the radiuses of pore i, j and throat; α is the pore-throat partition coefficient of the pore-throat interface and is taken as 0.6.

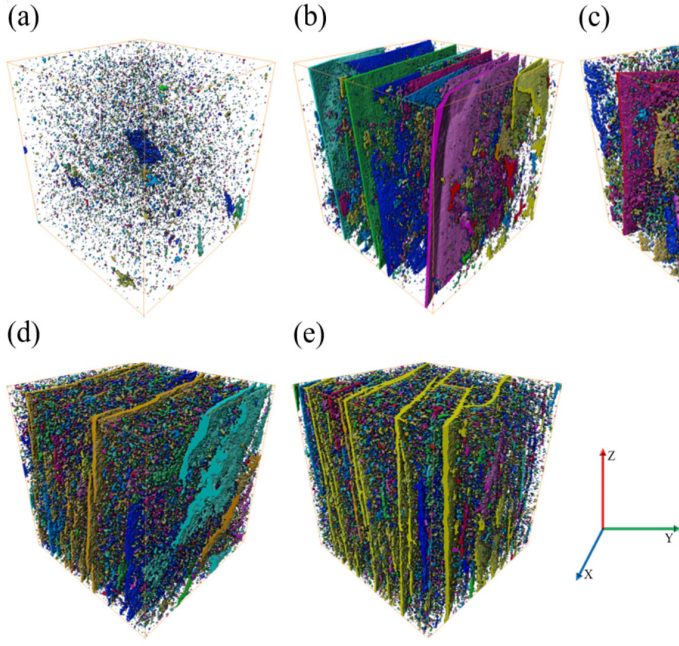

Fig. 4. Pores and fractures at different microwave temperatures: (a) 25 °C; (b) 350 °C; (c) 400 °C; (d) 500 °C; (e) 600 °C.

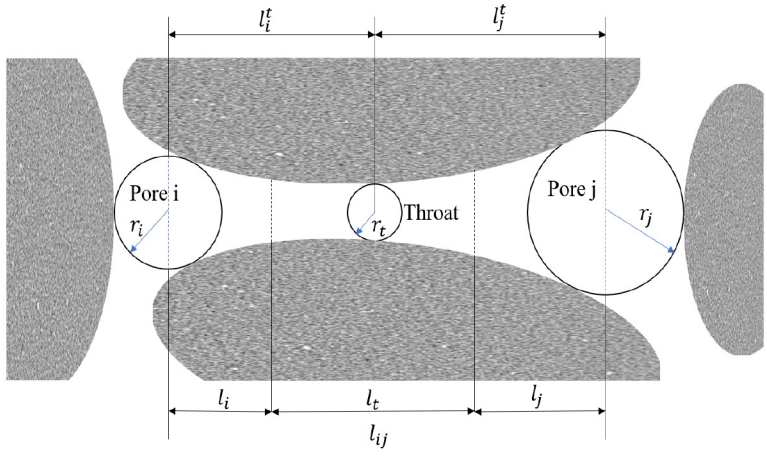

Fig. 5. Schematic diagram of the pore-throat channel construction.

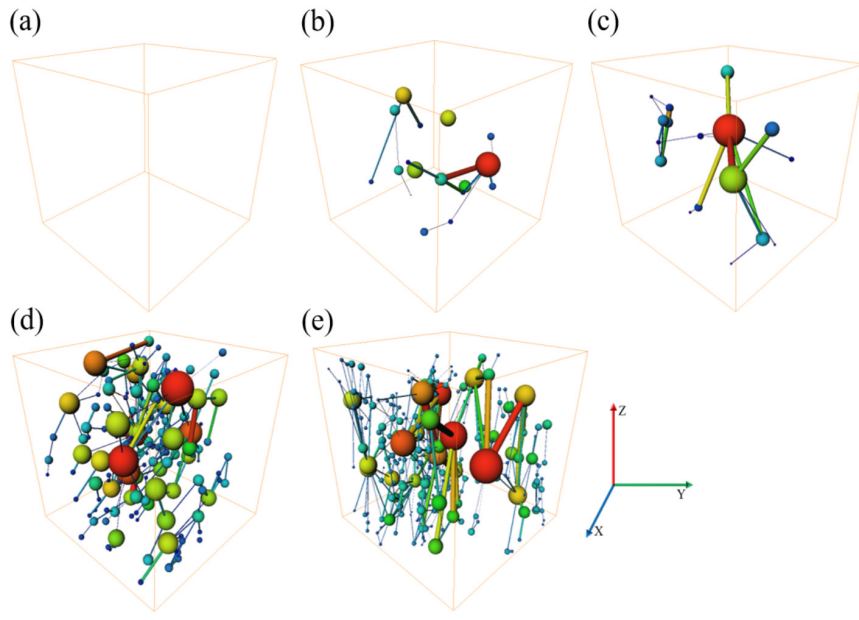

Fig. 6. The equivalent ball and stick model at different temperatures: (a) 25 °C; (b) 350 °C; (c) 400 °C; (d) 500 °C; (e) 600 °C. The colors of the balls (pore cavities) and rod (fractures) denote their equivalent volume.

3. Results and discussion

3.1. Rock thermal fracture analysis

Figures 2a and 2b show that in the first stage of heating from ambient to 350 °C, oil shale gradually undergoes thermal cracking due to thermal radiation. The volumetric heating advantage of microwave radiation, heat transfer and heat exchange start in the OM-rich area inside the oil shale sample. Water contained within the rock has highly dielectric properties, and is rapidly heated by the microwaves, generating steam inside oil shale, which leads to the separation of the layers that form its structure. The effect of the thermal expansion of particles of different density becomes obvious, as stress tends to be concentrated around hard mineral particles, developing fractures and cracks along the laminae. Although this alone increases permeability, at these temperatures the pyrolysis of kerogen is incomplete and the hydrocarbon content increases only slowly.

In the second stage (400–500 °C), a large number of cracks appear on the surface of oil shale and a large amount of oil and gas seeps out. This occurs for the following three main reasons.

First, as the microwave radiation time increases, the heat transfer efficiency within the rock also increases and the number and length of surface cracks increase significantly. The organic matter between the oil shale particles becomes an oil-like liquid, which, because of its higher microwave absorption potential, leads to a significant separation of the oil shale laminae. At 400 °C, due to the microwave irradiation resulting in the thermal expansion within oil shale and inorganic minerals (such as pyrite), which are very sensitive to the thermal response to temperature, thermal stress is often generated at the interface between different mineral components, resulting in a further expansion of the fracture, providing a larger channel for the transport of oil and gas (Fig. 2e). The low internal water content of oil shale has a significant impact on microwave heating, accelerating the process. At the stage from room temperature to the start of heating and desorption, the adsorbed water in oil shale and the interlayer water in the clay minerals are heated and evaporated by microwave radiation.

Second, as seen in Figure 2d, when the temperature reaches 500 °C, oil and gas start to accumulate on the sample surface; kerogen starts to pyrolyze in large quantities and generate liquid hydrocarbons, in addition to gases such as hydrogen and carbon dioxide, leading to the creation of pores and fractures inside oil shale. Moreover, during the process of shale oil and gas expulsion from the sample interior to its surface, a significant microfracture expansion occurs and the range of oil and gas seepage is enhanced.

Third, kerogen undergoes complex physical changes and chemical reactions at high temperatures. This demonstrates that seepage channels increase rapidly due to the combined effect of thermal fracture of the rock and pyrolysis of kerogen [35].

At 600 °C, the amount of released gas decreases, and oil and gas are completely expelled at this temperature. The color of the rock has changed from black at room temperature to earthy yellow (Fig. 2e). When the sample is volumetrically heated to this temperature, the oil shale sample is converted into shale oil and gas. The vapors and volatiles generate a high jet pressure within the rock matrix, causing the rapid fracture expansion and interconnection of mutually parallel fractures. Meanwhile, some water-bearing clay minerals are mainly present inside the oil shale sample. In this temperature range its internal crystalline water produces high temperature water loss at high temperatures.

Moreover, at high temperatures the number of oil and gas diffusion reactions increases, and oil and gas products are generated faster than they can diffuse out of pores and fractures. The coking of clay minerals due to the transport of hydrocarbons and secondary reactions of oil and gas reaches its maximum, in addition, the microwave radiation extends along the mechanically weak surface and generates a large number of fractures. Secondary coking involves reactions within the liquid oil and the fusion of two or more molecules to form the main carbonaceous products. For these reasons, microwave heating at 600 °C has the most effective outcome.

3.2. SEM experimental analysis

Figures 7a–e depict SEM images of shale oil at different temperatures and 800 W microwave power. The oil shale samples after microwave pyrolysis show oil and gas to have been completely discharged at 600 °C, and the gradual pyrolysis of cheese roots within the samples at high temperatures produces new pore fissures and clay minerals are chemically altered at such temperatures. So, 600 °C is the optimum temperature for oil and gas extraction, as discussed above. The SEM scans of the samples show the produced two-dimensional images of their surface morphology and the distribution of minerals. Electron beam sputtering plating displays the surface morphology of the oil shale samples in more detail, including the distribution of organic matter and the induced pores and fractures and their directions after microwave irradiation. SEM at 1000× magnification reveals clay minerals to be the most common minerals in oil shale. These minerals play an important role in the enrichment of organic matter and have a good linear correlation with it [36]. Therefore, the higher clay mineral content indicates a greater abundance of OM in oil shale. Clay minerals mainly contain kaolinite, montmorillonite, illite, etc. The reaction mechanism is more complicated at high temperatures, for example, kaolinite becomes metakaolinite at 600 °C when the internal hydroxyl group starts to be removed to bring about a crystalline transformation. This leads to the reduction in the internal strength of the rock, resulting in the loosening and disintegration of the matrix rock particles inside the rock.

In the microwave heating experiment, organic matter is gradually pyrolyzed with rising temperature. Figure 7 shows the organic matter in the rock to be of higher abundance at room temperature. The electron micrographs of oil shale reveal the presence of organic matter at room temperature, at the same time, pores and fissures cannot be observed, which indicates that oil shale is very dense at this temperature. As microwave heating time increases and temperature gradually rises, the OM content gradually decreases. At 350 °C, because the organic matter in various minerals is randomly dispersed, different minerals have different temperatures. When heated to 400 or 500 °C, pyrolysis of OM gradually begins (Fig. 7c–d). At these temperatures, it is mainly the physical properties of OM that undergo changes. The thermal decomposition process of organic matter in oil shale takes place in either one or two stages, depending on the type of the rock. In Fushun oil shale, kerogen decomposes into hot bitumen, which in turn decomposes into the final product. The randomly dispersed organic matter on the surface gradually begins to be pyrolyzed and the formerly OM-rich areas gradually become a smooth rock matrix. By 600 °C, the organic matter on the surface of the oil shale sample has been completely decomposed, as discussed above, and large pores and fissures have formed due to the jet effect of the ejected oil and gas (Fig. 7e). Meanwhile, the decomposition of carbonate minerals such as calcite and dolomite also promotes the generation of pore-fracture. In addition, the pyrite contained inside the oil shale sample is a strong microwave absorber

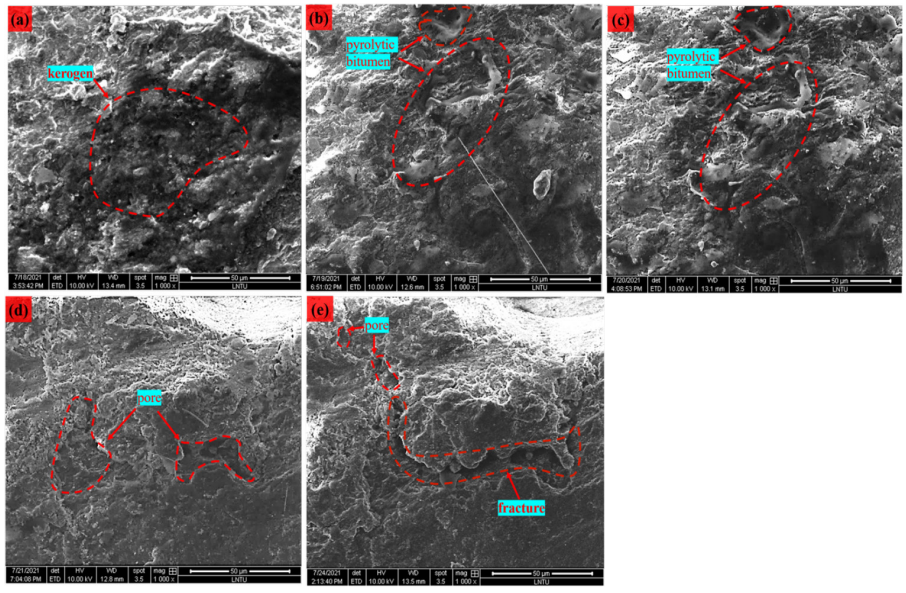

Fig. 7. SEM images of shale oil at different temperatures and 800 W microwave power: (a) 25 °C; (b) 350 °C; (c) 400 °C; (d) 500 °C; (e) 600 °C.

and can absorb heat rapidly under microwave radiation. Phase transformation occurs and with increasing temperature, pyrite will transform into hematite and magnetite. However, the content of pyrite in oil shale is relatively low and has a little effect on its heating. The distribution of the mineral fraction and kerogen is not uniform. This may affect the formation of the pore network inside the oil shale sample under microwave radiation [37].

3.3. Pore structure evolution visualization of oil shale pyrolysis process using μCT

In Figure 4 different colors are used to indicate pores, microfractures and fractures. Their random distribution throughout the rock mass has been caused by the uneven distribution of minerals, which leads to heterogeneous deformation during heating due to the differences in thermal expansion between the minerals present in various proportions. During pyrolysis, thermal cracking occurs to different extents in the rocks near different mineral fractions.

Because of the anisotropy of oil shale, high-density minerals differ in number and location in each sample. As discussed, inorganic minerals are shown to be white in the scan image; pores and fractures are black. Figures 4a–e illustrate the randomness, which reflects the material properties of the oil shale itself. When microwave heating is carried out, there is a discrepancy

between the coefficient of thermal expansion of the minerals and of the matrix material of the shale; fractures are therefore extremely likely to occur where mineral particles are present. When fractures propagate parallel to the bedding, internal fracturing also tends to develop in a direction roughly parallel to the bedding. Since the oil shale specimen is no longer constrained by surrounding stresses in the rock mass, fracturing due to microwave heating is more obvious. Microfractures occur in large numbers and tend to increase in size while large fractures are propagating. During heating, the coefficients of thermal expansion of inorganic mineral particles in the rock differ greatly from those of adjacent materials. Fractures are therefore highly likely to form at the edges of mineral grains during pyrolysis and mostly propagate in the laminae direction, while very few cracks form in the perpendicular direction. This is mainly due to the anisotropic strength of shale and its significantly higher resistance to the fracturing normal to the bedding.

Microwave heating produces temperature gradients in the oil shale sample and thermocouples determine its temperature only within a specific interval. The porosity at different temperatures is directly determined by a standardized image processing process. Due to the pyrolysis of dry caseous roots at high temperatures, the generation of shale oil and gas enlarges the pores during phase changes and the internal fractures gradually widen with temperature increasing. As seen from Figure 4b, at 350 °C the laminae gradually undergo thermal rupture at high temperatures. Organic matter absorbs the radiant energy along the fracture laminae inside the rock and many parallel fractures are scattered throughout the oil shale sample to form a more complete seepage channel. When the temperature reaches 400 °C, thermal cracking becomes more obvious and the number of internal microfractures increases. The microfractures produced by further heating bring more organic matter into contact with the external medium, thus increasing the production of shale oil.

At 500 °C, the thermal cracking and pyrolysis of organic matter display synergistic effects, resulting in the formation of a large number of pores inside the rock and increasing the fracturing gradually. The number of individual pores step-by-step increases with accelerating OM pyrolysis, while the fracturing of the rock increases significantly. Fractures continued to propagate and increase the permeability, but did not reach the peak value at this temperature.

By 600 °C, as noted above, many fractures had intersected to form a complete seepage channel and the appearance of connected pores was observed.

Because of the highly heterogeneous nature of oil shale, the connectivity is poor perpendicular to the laminae and strong parallel to the laminae. In order to visualize the porosity variation and connectivity of the laminae in oil shale, the porosity of the slice images was analyzed to reflect the change of porosity parallel and perpendicular to the laminae. Three-dimensional X-ray μCT was used to investigate the change of porosity of bituminous coal during the fracturing process. The original laminae were interconnected with isolated

pores after pressure had been applied, and the fractures were generated mainly from the laminae surface, thus enhancing the connectivity and permeability of coal [38].

The pores, microfractures and fractures were extracted from the sections, their spatial locations were ascertained and the porosity of each section was analyzed. Obvious penetration fractures were seen in the samples, while a large number of pore fractures formed a pore network and the highly connected seepage channels were present inside the samples.

Figure 8 shows the variation of porosity in the XY, XZ and YZ slice directions and total porosity. At 350 °C, the overall distribution of porosity was reasonably uniform, but larger pores are evident in the centre, appearing as a large peak (Fig. 8b). In the figure, the maximum slice porosity appears only parallel to the laminae direction, indicating a higher ratio of oil shale fractures as well as microfractures.

The maximum slice porosity at 25 °C was 1.47% (Fig. 8a). The maximum slice porosity at 350 °C was 11.77% (Fig. 8b), 8 times the value at 25 °C. At 400 °C, the maximum slice porosity was 14.29% (Fig. 8c), or 9.7 times the value at 25 °C. At the same time, at 500 °C, the maximum slice porosity reached 17.49% (Fig. 8d), which was 11.89 times the maximum slice porosity at 25 °C. At 600 °C, the slice porosity increased only slightly to 19.32% (Fig. 8e), which was 13.14 times the maximum slice porosity at 25 °C. The total porosity increased by a factor of 52.65, from the initial 0.26% to 13.69% at 600 °C (Fig. 8f). These results indicate that the caseous roots within the oil shale sample were all pyrolyzed at 500–600 °C and significantly increased porosity. The distribution of porosity is mainly affected by the transport of hydrocarbons, dehydration and decomposition of clay minerals and decomposition of small amounts of carbonates and silicates. In this temperature range, carbonates decompose carbon dioxide as well as water vapor due to the chemical reactions taking place at these temperatures owing to the excessive temperatures. Silicates promote the extension of fractures within the oil shale sample due to the hydration reactions, thus reducing the strength of the rock. These phenomena inevitably lead to a decrease in the density, thermal conductivity and mechanical properties of the rock, while at the same time its percolation properties are enhanced and the porosity and permeability increase significantly [39]. The degree of pyrolysis within the rock due to microwave heating was higher than that on the surface, indicating the advantage of volumetric heating by microwaves. The heating path of the shale was consistent with the direction of oil and gas discharge after volumetric heating, which facilitated their discharge. The other microfractures were joined with connecting pores to form an effective seepage channel.

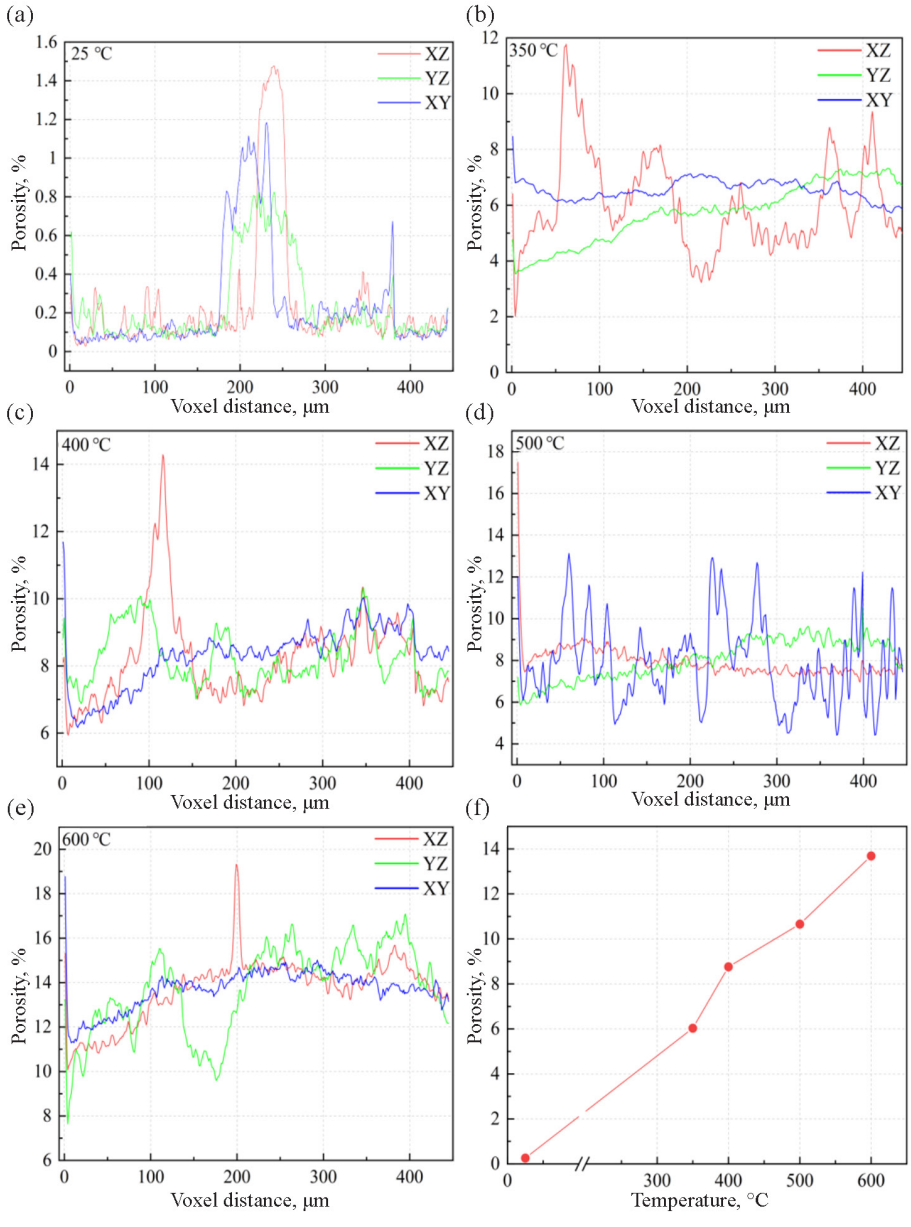

Fig. 8. Porosity and total porosity in different voxel directions at different temperatures: (a) 25 °C; (b) 350 °C; (c) 400 °C; (d) 500 °C; (e) 600 °C; (f) total porosity at different temperatures.

3.4. Pore-scale network model analysis

The pore-scale network model (PNM) was used to analyze the pores distribution in the oil shale sample. Inside the sample, the pore space consists both of connected and isolated pores. The volume of the connected pore space using the connectivity algorithm has been proposed earlier [40]. The ball and stick model depicted in Figure 6 is an example of a cross-linkage model consisting of pores and fractures calculated from the maximum sphere algorithm. The algorithm can effectively characterize the pore space and also retains the pore space distribution characteristics of the original core images. The "balls" and "throats" in the pore network model are determined by finding the local maximum as well as minimum ball between the maximum balls in a two-dimensional space. The density of pores and fractures determines the oil and gas transport paths within the oil shale sample, and also its output efficiency. At normal temperature, there are only a few pores inside the sample, which cannot form a complete seepage channel, and there are only isolated pores inside it without connecting pores, which cannot form a complete equivalent sphere or channel in the equivalent spherical stick model. With increasing temperature, the corresponding connecting pores and penetrating fractures are produced inside, which provides favorable conditions for the pyrolysis of cheese roots and the transport of oil and gas. The pattern of that model is similar to the microstructure morphology structure proposed by Blunt et al. earlier [41]. Qualitatively, the connectivity of this equivalent model is significantly enhanced by microwave radiation. The number and connectivity of cross-linked micropores and fissures increase substantially, facilitating the accumulation of hydrocarbons.

The histograms in Figure 9 and Figure 10 show the equivalent pore and throat length dimensions determined by the pore network model at 350–600 °C to be mainly between 10 and 20 μm. It is clear from these figures that the pores became more completely connected at higher temperatures, and larger equivalent spheres were formed. At 500 °C the percentage of pores with a diameter smaller than 10 μm peaked and the percentage of pores in the 10–20 μm diameter range slightly decreased. At 600 °C the percentage of pores with < 10 μm diameter suddenly dropped, pores with a diameter > 50 μm appeared and the connectivity of the pore space increased. The lower percentage of smaller pores indicates a greater overall pore volume.

Last but not least, the microscopic morphology to be addressed is the throat structure. The distribution and number of channels connecting the pores determine the ease of fluid transport within the microstructure. The number of channels with diameters up to 100 μm increased significantly with rising temperature, and new channels formed in previously impermeable areas, along with the transport of oil and gas. The percentage of channel lengths did not increase significantly from 500 °C to 600 °C. With increasing average pore radius and number of throat channels, the pore network is gradually developed to completeness. The increase of connected pores directly leads

to the increase of equivalent pores, the pore space becomes more complete in the whole network and the interconnected pores form more interconnected throats. To this extent, PNM reflected actual pore space changes in the oil shale sample pyrolyzed by microwave radiation.

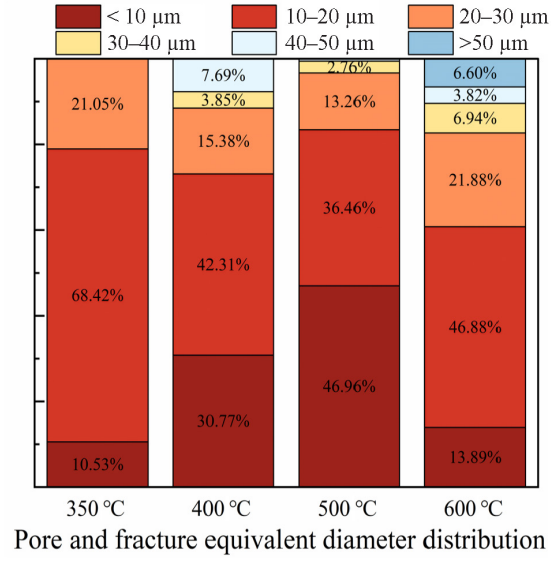

Fig. 9. Histogram of equivalent pore and fracture diameters at different temperatures.

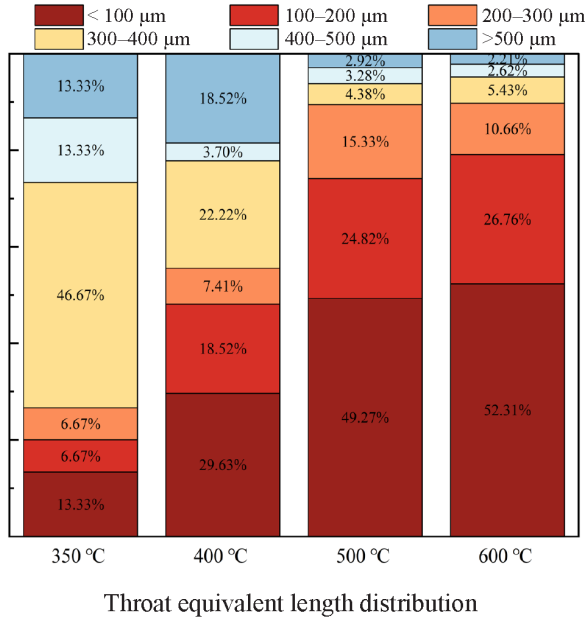

Fig. 10. Histogram of equivalent throat lengths at different temperatures.

4. Conclusions

In this study, the effects of different pyrolytic temperatures on the heating behavior, surface morphology and internal spatial structure of pores and fractures in Fushun oil shale were investigated at a microwave power of 800 W. The pore and fracture structure and distribution in oil shale were investigated by microwave pyrolysis experiments, scanning electron microsopy and microcomputed tomography scans, and computed tomography post-processing. The following conclusions were drawn.

Oil shale is dense at room temperature, while its non-homogeneity gradually increases with rising pyrolysis temperature. Oil shale produces a large number of internal pore fractures and gradually its non-homogeneity becomes significant. These observations show that the increase of reaction temperature resulted in the increase of internal pressure generated by water vapor and volatiles as well as the thermal stress caused by microwave radiation, induced the generation of pore fractures and formed a network of oil and gas seepage channels inside the matrix of the rock.

Microwave radiation, which causes mainly volumetric heating, gradually decreased the kerogen content with increasing temperature. Porosity increased from 0.26% at room temperature to 13.69% at 600 °C, increase being 52.65 times the initial porosity. A 19.32% peak value of surface porosity (13.14 times the maximum porosity at room temperature) was observed at 600 °C. It is proved that oil shale is sufficiently pyrolyzed at 600 °C, which is the optimal choice in the microwave pyrolysis state.

The above analysis has implications for the application of microwave heating in oil shale development. However, due to the inability to observe at a nanoscale or even from a sub-micron microscopic perspective, this paper lacks an assessment of the accuracy of the multi-scale studies described. This factor should be fully considered in future studies.

Acknowledgments

This study was supported by the Liaoning Provincial Department of Education General Project (Grant Nos. LJKZ0360, LJKZ0329) and by the Discipline Innovation Team Project of Liaoning Technical University (Grant No. LNTU20TD-11).

The publication costs of this article were partially covered by the Estonian Academy of Sciences.

REFERENCES

1. Russell, P. L. World history and resources of oil shale. *Energy Explor. Exploit.*, 1986, **4**(4), 301–320.
2. Wang, M., Ma, R., Li, J., Lu, S., Li, C., Guo, Z., Li, Z. Occurrence mechanism of lacustrine shale oil in the Paleogene Shahejie Formation of Jiyang depression, Bohai Bay Basin, China. *Pet. Explor. Dev.*, 2019, **46**(4), 833–846.
3. Lu, S., Huang, W., Chen, F., Li, J., Wang, M., Xue, H., Wang, W., Cai, X. Classification and evaluation criteria of shale oil and gas resources: Discussion and application. *Pet. Explor. Dev.*, 2012, **39**(2), 268–276.
4. Li, S., Yue, C. Study of pyrolysis kinetics of oil shale. *Fuel*, 2003, **82**(3), 337–342.
5. Li, S., Yue, C. Study of different kinetic models for oil shale pyrolysis. *Fuel Process. Technol.*, 2004, **85**(1), 51–61.
6. Kök, M. V., Guner, G., Bagci, S. Laboratory steam injection applications for oil shale fields of Turkey. *Oil Shale*, 2008, **25**(1), 37–46.
7. Chanaa, M. B., Lallemant, M., Mokhlisse, A. Pyrolysis of Timahdit, Morocco, oil shales under microwave field. *Fuel*, 1994, **73**(10), 1643–1649.
8. Lin, L., Lai, D., Guo, E., Zhang, C., Xu, G. Oil shale pyrolysis in indirectly heated fixed bed with metallic plates of heating enhancement. *Fuel*, 2016, **163**, 48–55.
9. Wang, G., Liu, S., Yang, D., Fu, M. Numerical study on the in-situ pyrolysis process of steeply dipping oil shale deposits by injecting superheated water steam: A case study on Jimsar oil shale in Xinjiang, China. *Energy*, 2022, **239**, 122182.
10. Meisels, R., Toifl, M., Hartlieb, P., Kuchar, F., Antretter, T. Microwave propagation and absorption and its thermo-mechanical consequences in heterogeneous rocks. *Int. J. Miner. Process.*, 2015, **135**, 40–51.
11. Kumar, H., Lester, E., Kingman, S., Bourne, R., Avila, C., Jones, A., Robinson, J., Halleck, P. M., Mathews, J. P. Inducing fractures and increasing cleat apertures in a bituminous coal under isotropic stress via application of microwave energy. *Int. J. Coal Geol.*, 2011, **88**(1), 75–82.
12. Bradhurst, D. H., Worner, H. K. Evaluation of oil produced from the microwave retorting of Australian shales. *Fuel*, 1996, **75**(3), 285–288.
13. Jesch, R. L., McLaughlin, R. H. Dielectric measurements of oil shale as functions of temperature and frequency. *IEEE Trans. Geosci. Remote Sens.*, 1984, **GE-22**(2), 99–105.
14. Hascakir, B., Akin, S. Recovery of Turkish oil shales by electromagnetic heating and determination of the dielectric properties of oil shales by an analytical method. *Energy Fuels*, 2010, **24**(1), 503–509.
15. Zhang, N., He, M., Zhang, B., Qiao, F., Sheng, H., Hu, Q. Pore structure characteristics and permeability of deep sedimentary rocks determined by mercury intrusion porosimetry. *J. Earth Sci.*, 2016, **27**(4), 670–676.
16. Wang, G., Jiao, G., Liu, H., Bai, J., Li, S. Variation of the pore structure during microwave pyrolysis of oil shale. *Oil Shale*, 2010, **27**(2), 135–146.
17. Kang, Z., Zhao, J., Yang, D., Zhao, Y., Hu, Y. Study of the evolution of micron-

scale pore structure in oil shale at different temperatures. *Oil Shale*, 2017, **34**(1), 42–54.
18. Han, X., Jiang, X., Yu, L., Cui, Z. Change of pore structure of oil shale particles during combustion. Part 1. Evolution mechanism. *Energy Fuels*, 2006, **20**(6), 2408–2412.
19. Han, X., Jiang, X., Cui, Z. Change of pore structure of oil shale particles during combustion. 2. Pore structure of oil-shale ash. *Energy Fuels*, 2008, **22**(2), 972–975.
20. Xu, S., Sun, Y., Lü, X., Yang, Q., Li, Q., Wang, Z., Guo, M. Effects of composition and pore evolution on thermophysical properties of Huadian oil shale in retorting and oxidizing pyrolysis. *Fuel*, 2021, **305**, 121565.
21. Wu, W., Wang, G., Liu, G., Dong, X., Yu, J., Pan, J. Micron-nano pore structures and microscopic pore distribution of oil shale in the Shahejie Formation of the Dongying Depression, Bohai Bay basin, using the argon-scanning electron microscope method. *J. Nanosci. Nanotechnol.*, 2021, **21**(1), 750–764.
22. Bai, B., Elgmati, M., Zhang, H., Wei, M. Rock characterization of Fayetteville shale gas plays. *Fuel*, 2013, **105**, 645–652.
23. Bian, H., Xia, Y., Lu, C., Qin, X., Meng, Q., Lu, H. Pore structure fractal characterization and permeability simulation of natural gas hydrate reservoir based on CT images. *Geofluids*, **2020**, Article ID 6934691.
24. Wang, L., Yang, D., Kang, Z. Evolution of permeability and mesostructure of oil shale exposed to high-temperature water vapor. *Fuel*, 2021, **290**, 119786.
25. Cao, G., Lin, M., Ji, L., Jiang, W., Yang, M. Characterization of pore structures and gas transport characteristics of Longmaxi shale. *Fuel*, 2019, **258**, 116146.
26. Zhang, L., Chen, S., Zhang, C., Fang, X., Li, S. The characterization of bituminous coal microstructure and permeability by liquid nitrogen fracturing based on μCT technology. *Fuel*, 2020, **262**, 116635.
27. Chen, L., He, A., Zhao, J., Kang, Q., Li, Z.-Y., Carmeliet. J., Shikazono, N., Tao, W.-Q. Pore-scale modeling of complex transport phenomena in porous media. *Prog. Energy Combust. Sci.*, 2022, **88**, 100968.
28. Hsieh, J., Molthen, R. C., Dawson, C. A., Johnson, R. H. An iterative approach to the beam hardening correction in cone beam CT. *Med. Phys.*, 2000, **27**(1), 23–29.
29. Karimpouli, S., Tahmasebi, P., Saenger, E. H. Coal cleat/fracture segmentation using convolutional neural networks. *Nat. Resour. Res.*, 2020, **29**(3), 1675–1685.
30. Wang, S., Chen, Z., Zhang, M. Pore and microfracture of coal matrix block and their effects on the recovery of methane from coal. *Earth Science-Journal of China University of Geosciences*, 1995, **20**(5), 557–561 (in Chinese).
31. Otsu, N. A threshold selection method from gray-level histograms. *IEEE Trans. Syst. Man Cybern.*, 1979, **9**(1), 62–66.
32. Rodriguez, F., Maire, E., Courjault-Radé, P., Darrozes, J. The Black Top Hat function applied to a DEM: A tool to estimate recent incision in a mountainous watershed (Estibère Watershed, Central Pyrenees). *Geophys. Res. Lett.*, 2002, **29**(6), 9–1–9–4.

33. Saif, T., Lin, Q., Bijeljic, B., Blunt, M.J. Microstructural imaging and characte rization of oil shale before and after pyrolysis. *Fuel*, 2017, **197**, 562–574.
34. Dong, H., Blunt, M.J. C. Pore-network extraction from micro-computerized-tomography images. *Phys. Rev. E*, 2009, **80**(3), 036307.
35. Williams, P. T., Ahmad, N. Influence of process conditions on the pyrolysis of Pakistani oil shales. *Fuel*, 1999, **78**(6), 653–662.
36. Liu, Z., Meng, Q., Dong, Q., Zhu, J., Guo, W., Ye, S., Liu, R., Jia, J. Characteristics and resource potential of oil shale in China. *Oil Shale*, 2017, **34**(1), 15–41.
37. Wang, Q., Sun, B., Hu, A., Bai, J., Li, S. Pyrolysis characteristics of Huadian oil shales. *Oil Shale*, 2007, **24**(2), 147–157.
38. Akhondzadeh, H., Keshavarz, A., Al-Yaseri, A. Z., Ali, M., Awan, F. U. R., Wang, X., Yang, Y., Iglauer, S., Lebedev, M. Pore-scale analysis of coal cleat network evolution through liquid nitrogen treatment: A Micro-Computed Tomography investigation. *Int. J. Coal Geol.*, 2020, **219**, 103370.
39. Shang, H., Yue, Y., Zhang, J., Wang, J., Shi, Q., Zhang, W., Liu, L., Omar, S. Effect of microwave irradiation on the viscosity of crude oil: A view at the molecular level. *Fuel Process. Technol.*, 2018, **170**, 44–52.
40. Wu, Y., Lin, C., Ren, L., Yan, W., An, S., Chen, B., Wang, Y., Zhang, X., You, C., Zhang, Y. Reconstruction of 3D porous media using multiple-point statistics based on a 3D training image. *J. Nat. Gas Sci. Eng.*, 2018, **51**, 129–140.
41. Blunt, M. J., Bijeljic, B., Dong, H., Gharbi, O., Iglauer, S., Mostaghimi, P., Paluszny, A., Pentland, C. Pore-scale imaging and modelling. *Adv. Water Resour.*, 2013, **51**, 197–216.